Available online at www.sciencedirect.com

jmr&t
Journal of Materials Research and Technology
www.jmrt.com.br

Original Article

Modification of Al-10Si-2Cu alloy surface by intensive pulsed electron beam

Sergey Konovalov [a,b,c,*], *Dmitrii Zaguliaev* [a,b], *Yurii Ivanov* [d], *Victor Gromov* [b], *Anna Abaturova* [b]

[a] *Wenzhou University Institute of Laser and Optoelectronic Intelligent Manufacturing, Wenzhou 325024, China*
[b] *Siberian State Industrial University, Novokuznetsk 654007, Russia*
[c] *Samara National Research University, Samara 443086, Russia*
[d] *Institute of High Current Electronics of the Siberian Branch of the RAS, Tomsk 634055, Russia*

ARTICLE INFO

Article history:
Received 28 February 2020
Accepted 21 March 2020
Available online 1 May 2020

Keywords:
Al-10Si-2Cu alloy
Silumin
Electron beam processing
Microstructure
Microhardness

ABSTRACT

The study reports on the electron-beam processing (energy of accelerated electrons 17 keV, electron beam energy density $E_S = 10$, 20, 30, 40, and 50 J/cm^2, pulse duration 50 and 200 μs) of Al-10wt%Si-2wt%Cu alloy (silumin) surface. The important outcome to emerge from the study is a correlation between surface microhardness and electron beam energy density. As revealed, a maximal microhardness value is at $E_S = (30–40)$ J/cm^2, being more than 1.6 times higher than the characteristic of the untreated material. The research has pointed out the electron-beam processing of silumin at $E_S = 10$ J/cm^2 causes the intensive destruction and microcracking along grain boundaries with particles of intermetallic compounds, as well as the globularization of cementite lamellae in eutectics. The irradiation of silumin by an electron beam ($E_S = 30–50$ J/cm^2) is shown to bring about the origination of micropores in the surface of samples, the dissolution of silicon, the globularization of intermetallic inclusions; in addition, a sub-micro-sized crystal structure of high-speed cellular crystallization forms. Finally, the electron-beam processing of silumin leads to the saturation of Al-based crystal lattice with alloying and impurity elements.

1. Introduction

The effect of high-energy high-current electron beams and laser shock processing represents future efficient methods to modify the surface in metals and alloys. Their major advantage over the alloying is better energy absorption instead of the introducing other impurities [1–24]. The laser shock-wave treatment of materials allows obtaining the preset physical and chemical properties of the surface and is promising for surface hardening of steels with a view to increasing their wear resistance, corrosion resistance and impact toughness [22–24]. A pulsed character of melting makes it possible to dissolve second phase particles, and non-equilibrium structure-phase states form in the molten surface owing to the rapid cooling (10^8–10^9 K/s) from a liquid state [2–7]; furthermore, the high-speed solidification results in a structure with

* *Corresponding author.*
E-mails: ksv@ssau.ru, ksv@wzu.edu.cn (S. Konovalov).
https://doi.org/10.1016/j.jmrt.2020.03.083

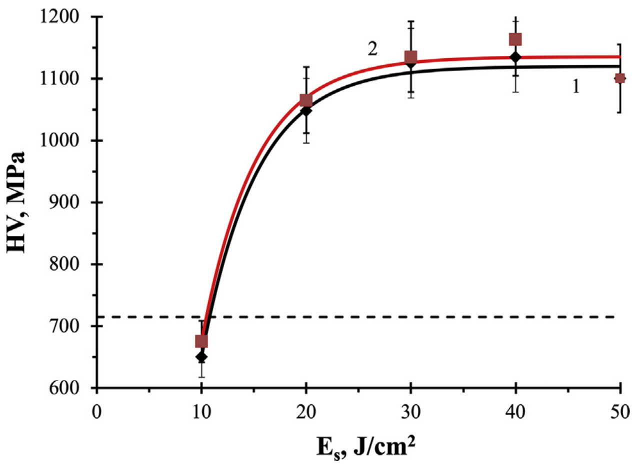

Fig. 1 – Microhardness of the irradiated alloy Al-10wt%Si-2wt%Cu surface vs. beam energy density for pulses of 50 μs (Curve 1) and 200 μs (Curve 2); an indenter loaded 1 N. A dotted line refers to the microhardness of as delivered silumin.

solid solutions, nano-dimensional second-phase segrations, and amorphous phase particles [8,9]. It is the ultrafast thermal cycles that allow using the electron-beam processing to increase hardness, wear and corrosion resistance [10–12]. The electron beam effect on the metal surface initiates diffusion processes. For instance, the electron irradiation of low-carbon steel causes the strong carbon diffusion and the formation of a solid solution Fe(C) on the surface of an over-saturated phase. The action of electron beams and solidification related to the cooling lead to the significant plastic deformation, which, in its turn, generates dislocation cells and amorphous structure. Interestingly, there is still no consensus on the effect of the electron-beam processing on transformations in a grain structure. Studies [13–16] have reported on the refinement of a grain structure up to the submicron range, whereas the other research [17–20] has revealed the grain growth in an alloy based on Al-Cu-Mg subjected to the electron irradiation.

Electron-beam processing is a broadly used technique to modify surfaces in a variety of metallic materials, i.e. Al-Si alloys; silumin is one of them. This alloy is a key material in motor car and aircraft production, mainly, for the casting air brakes, wheel housings, gear boxes and compressors, cylinder ends, pistons, and other motor elements. These alloys are materials with good castability, corrosion and heat resistance, machinability, electrical and heat conductivity, low density, heat extension, and low compression in casting. Al-Si alloys possess best strength properties among light alloys [25–31]. Nevertheless, despite such outstanding properties full-scale industrial use of these alloys experiences difficulties nowadays. Therefore, to improve surface properties of the material, it was subjected to the electron-beam processing, and research was carried out to reveal the effect of an intensive pulsed electron beam on the element and phase composition, a defect sub-structure state and microhardness in the surface of Al-10Si-2Cu alloy.

2. Material and methods of research

For the purpose of research, we used samples of Al-10wt%Si-2wt%Cu alloy (silumin) (chemical composition: 10.65 – Si; 2.11 – Cu; 0.89 – Ni; 0.85 – Mg; 0.26 – Fe; 0.03 – Mn; 0.05 – Ti; 0.01 – Pb; 0.02 – Zn; 0.01 – Cr; balanced by Al, wt.%). To carry out the electron irradiation, samples with a size of 10 mm in length, 10 mm in width, and 5 mm in height were made of as cast block. Prior to processing, samples were grinded and polished using a diamond suspension. A high-current pulsed electron beam was generated by an electron gun – a part of a laboratory unit “SOLO”. Operation parameters of this unit are thoroughly described in works [32,33]. Within this study characteristics of an electron beam were set as follows: energy of accelerated electrons 17 keV, electron beam energy density 10, 20, 30, 40, and 50 J/cm^2, pulse duration 50 and 200 μs, number of pulses 3, pulse repetition rate 0.3 s^{-1}; pressure of residual gas (argon) in the processing chamber of the unit $2{\cdot}10^{-2}$ Pa. The electron beam was oriented along the normal line to the sample surface, and a beam diameter was set to cover the whole sample surface. 5 samples were treated in each mode of electron beam irradiation. The samples were used for further tests and research. Data obtained were averaged and processed statistically.

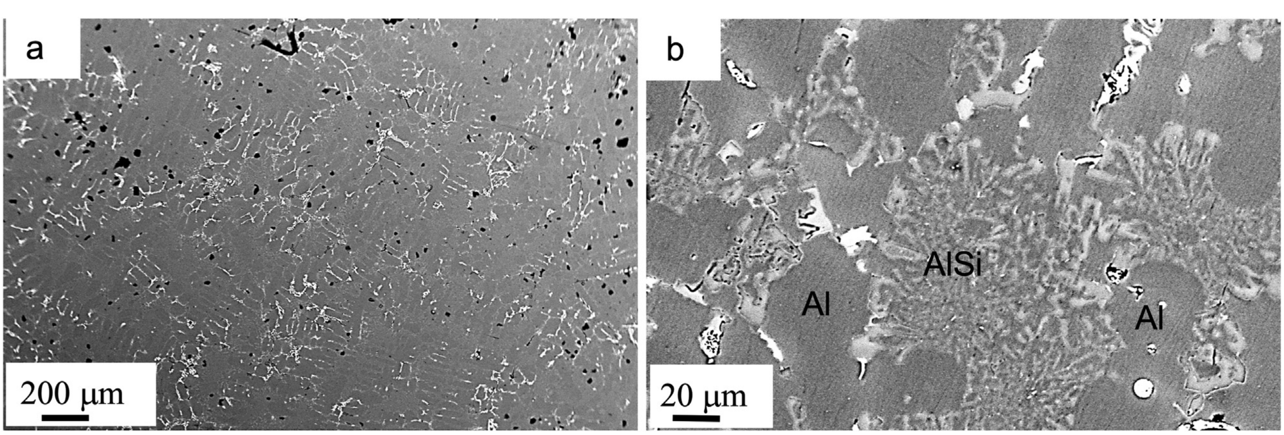

Fig. 2 – Structure of the destructed surface in as delivered silumin (prior to electron irradiation). Symbols (b): Al – aluminum grain; AlSi – eutectic grain.

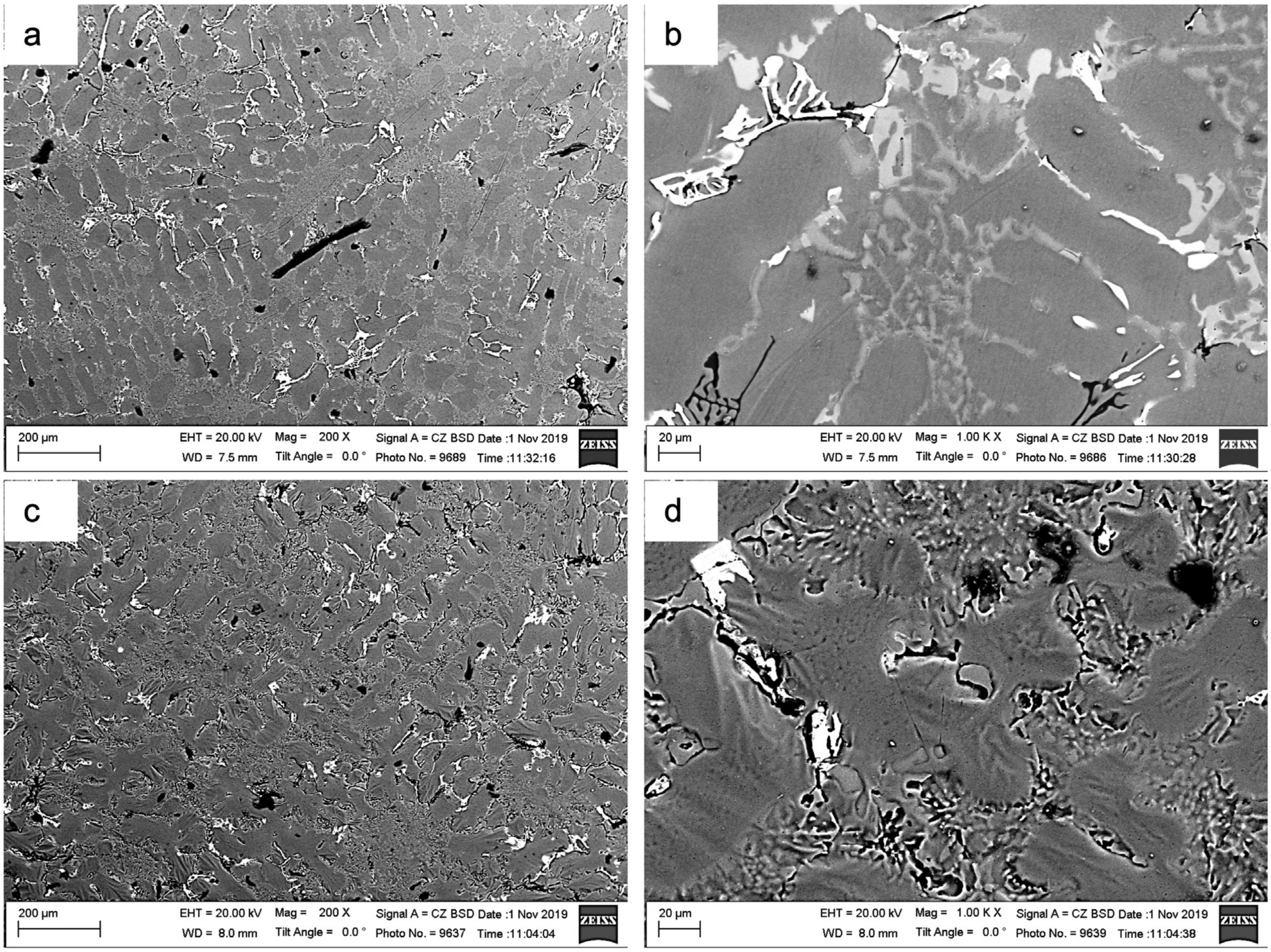

Fig. 3 – Silumin surface processed by a pulsed electron beam in conditions: a, b – 10 J/cm^2, 200 μs; c, d – 10 J/cm^2, 50 μs.

The element and phase composition, and the defect substructure state were analyzed with the help of scanning electron microscopy (Philips SEM-515 tooled with a microanalyzer EDAX ECON IV) and X-ray diffraction analysis (X-ray diffraction meter Shimadzu XRD 6000). 3 measurements of structure parameters were carried out for each sample. Figures demonstrate most typical views of the structure. Mechanical properties were characterized in terms of microhardness measured by microhardness tester HVS-1000, an indenter loaded 1 N (10 indentations with every sample were examined to determine confidence intervals and an average value of microhardness).

3. Results and discussion

Fig. 1 provides the research data on the microhardness of Al-10wt%Si-2wt%Cu alloy surface irradiated by a pulsed electron beam. It is apparent from the data that the microhardness of silumin surface increases in combination with the rising beam energy density E_S independently on the pulse duration. At E_S = 30–40 J/cm^2 it is maximal, being more than 1.6 times higher than this characteristic of the untreated material. In prior works we have found a 1.6 times increase in microhardness under other conditions of the electron-beam processing [34,35].

A surface structure of as delivered (not irradiated) Al-10wt%Si-2wt%Cu alloy samples and samples processed by a pulsed electron beam was analyzed by the methods of scanning electron microscopy. SEM data demonstrate that the alloy of interest in the as delivered state represents a polycrystalline aggregate to consist of grains of an aluminum-based solid solution (Fig. 2) and grains of eutectics AlSi (Fig. 2, b, eutectic grains are indicated AlSi).

The size of aluminum grains varies from 25 μm to 70 μm; AlSi eutectic grains are in a range from 55 μm to 80 μm. We found intermetallic inclusions with a variety of physical configurations in the structure of silumin ("Chinese hieroglyphs", needles, globules, lamellae) (Fig. 2, a). The biggest part of intermetallic inclusions was detected along grain boundaries, affecting their size this way.

The irradiation of silumin by an intensive pulsed electron beam is related to numerous transformations in the surface structure of samples. Given that an electron beam energy density is 10 J/cm^2, we observe intensive destructing and microcracking along grain boundaries, which contain intermetallic compounds (Fig. 3). Particles of intermetallic compounds fail to dissolve (Fig. 3). If an impulse lasts 50 μs,

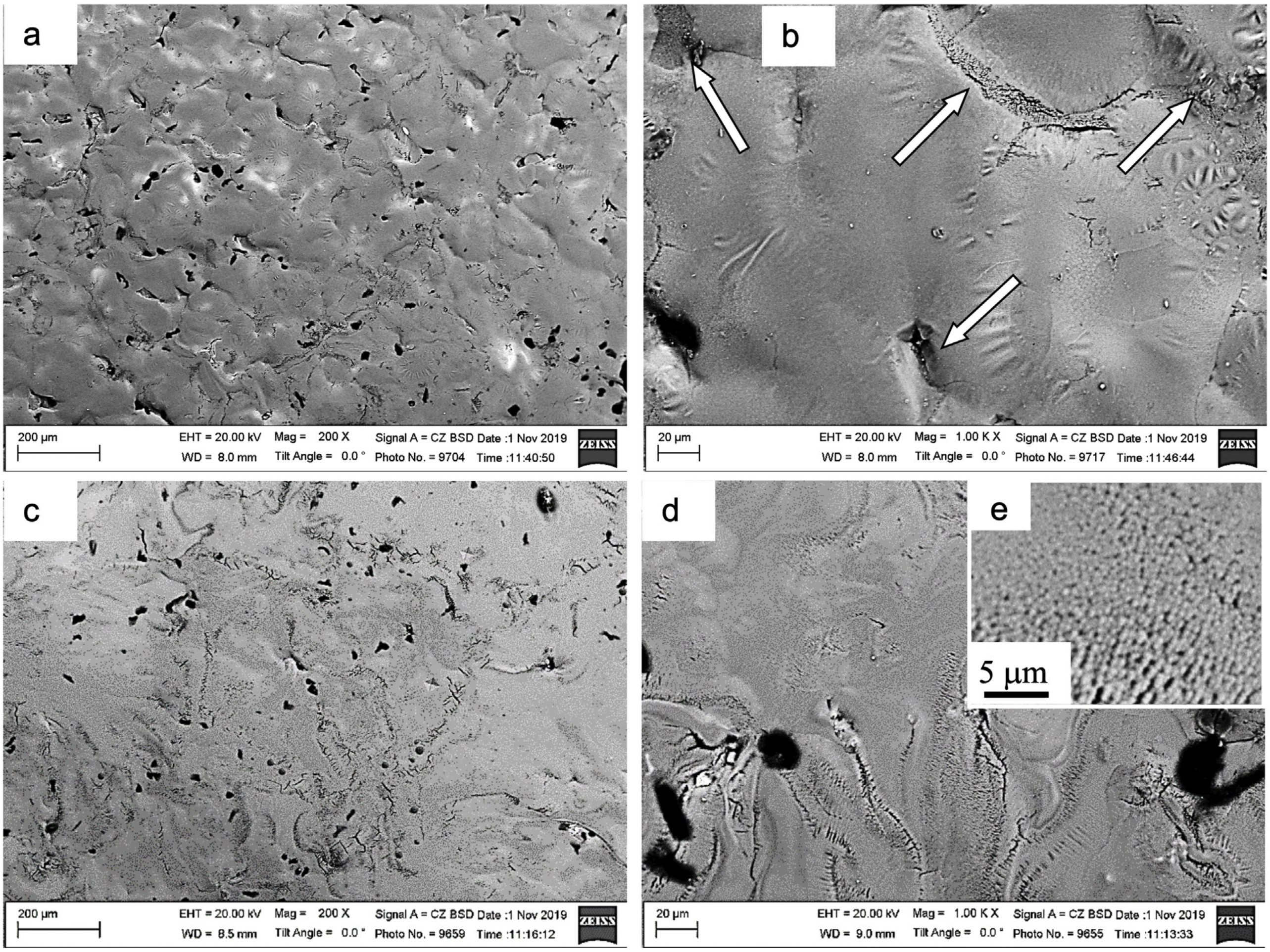

Fig. 4 – Structure of silumin surface exposed to the electron beam irradiation in conditions: a, b – 30 J/cm^2, 200 µs; c, d, e – 30 J/cm^2, 50 µs. Arrows (b) indicate a thin layer of the second phase along grain boundaries.

wavy topography tends to form in the volume of grains, indicating, probably, the first phase of melting in these material zones (Fig. 3, d). The irradiation of silumin is related to the splitting up of silicon lamellae in eutectic grains into globules. This process is particularly evident for an impulse of 50 µs.

The raise of a beam energy density up to 30 J/cm^2 initiates the formation of numerous micropores in the silumin surface (Fig. 4); a pulse time has no effect on their number and dimensions. Micropores might develop due to the material shrinkage under its high-speed crystallization related to the pulsed treatment of a material.

With no regard to a pulse time intermetallic compounds and silicon dissolve provided that silumin is irradiated with an electron beam energy density of 30 J/cm^2. Lengthy thin layers form along grain boundaries, where intermetallic inclusions are found. These thin layers are made of round particles with a size of 0.5–0.6 µm. When processing silumin by a pulsed electron beam (30 J/cm^2, 50 µs), sub-micro-sized crystal structure is detected in the volume of grains, crystallites 0.3–0.4 µm (Fig. 4, e).

Chaotically located microcracks are detected on the irradiated surface at a beam energy density of 50 J/cm^2, irrespectively to the pulse time (Fig. 5). The microcracking results from tensile stresses to develop in the surface layer of the material because of rapidly cooling surface to crystallize on an integrally cold base. The formation of a surface layer is related to the evolution of a high-speed structure of cellular crystallization, independently on the pulse time (Fig. 5, b, d). The size of cells is in a range of 500–650 nm.

An X-ray microanalysis was carried out to research the element composition in the silumin surface processed by an electron beam. Energy spectra (Fig. 6, b) were obtained on marked zones of the sample surface (Fig. 6, a). Table 1 presents data of X-ray microanalysis in the zone shown in Fig. 6, a; and Table 2 provides data relevant for all samples.

From the data given in Table 2 it is apparent there is a significant difference in a percentage of silicon determined in the course of an X-ray microanalysis in as delivered silumin samples and in those irradiated at a beam energy density of 10 J/cm^2. As a result of silumin electron irradiation in the high-speed melting mode of the surface (30 J/cm^2 and 50 J/cm^2), a structure forms with a percentage of silicon similar to the as delivered state. The silicon percentage in silumin determined in the X-ray microanalysis is supposed to depend on dimensions of silicon crystals. A longitudinal size of silicon lamellae is up to 10 µm, and a crosswise size ranges up to 1–1.5 µm in

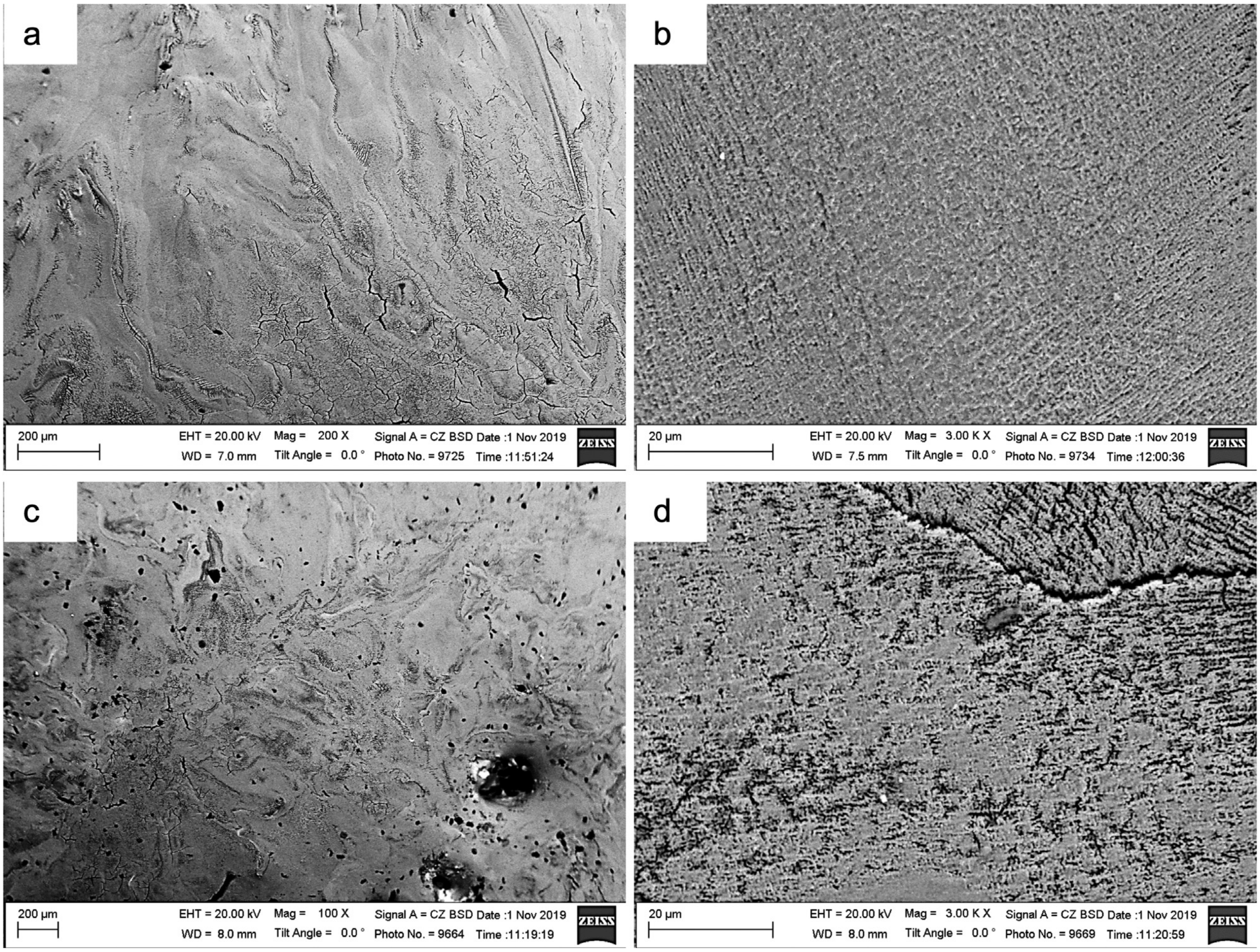

Fig. 5 – Structure of silumin surface irradiated by an electron beam in conditions: a, b – 50 J/cm^2, 200 μs; c, d – 50 J/cm^2, 50 μs.

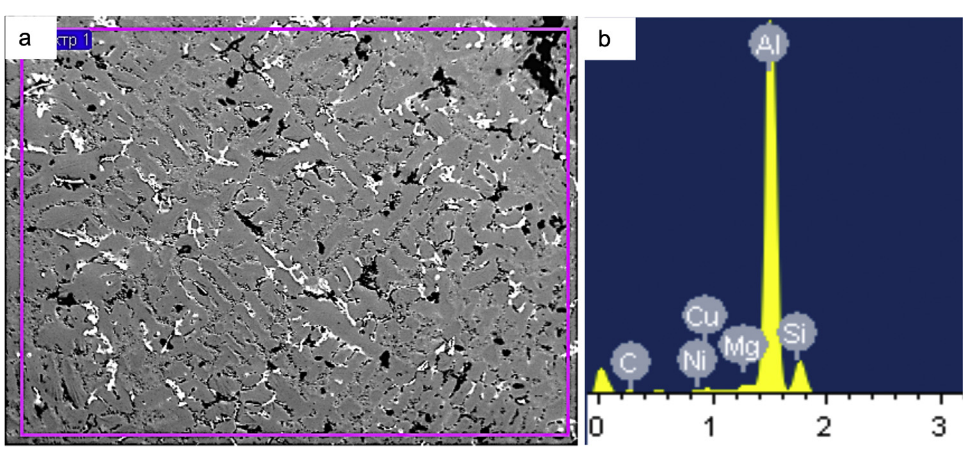

Fig. 6 – Electron-microscopic view of the irradiated sample surface (30 J/cm^2, 50 μs) (a); b – energy spectra obtained on the zone marked in (a).

as cast silumin and in the material irradiated by an electron beam at an energy density of 10 J/cm^2. The electron irradiation of silumin at an energy density of 30 J/cm^2 and higher initiates the dissolution of silicon lamellae and the re-release of globular particles (up to 100 nm) [36].

The phase composition in the silumin surface modified by an electron beam was investigated by the methods of X-ray crystallography. The analysis has pointed out principal phases in the as delivered material are a solid Al-based solution, silicon, and intermetallic compounds, i.e. phases $Fe_2Al_9Si_2$ and

Table 1 – Data products of spectra (Fig. 6, b). Number of iterations 4.

Element	Wt. %	At. %
Mg K	0.81	0.93
Al K	76.66	79.39
Si K	17.53	17.44
Ni K	1.22	0.58
Cu K	3.78	1.66
Total	100	

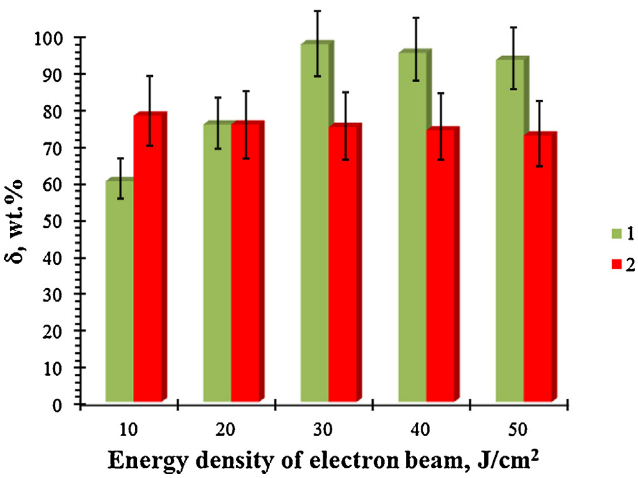

Fig. 7 – Percentage of Al-based solid solution in the silumin surface irradiated by a pulsed electron beam (1 – pulse time 200 μs; 2 – 50 μs) vs. beam energy density.

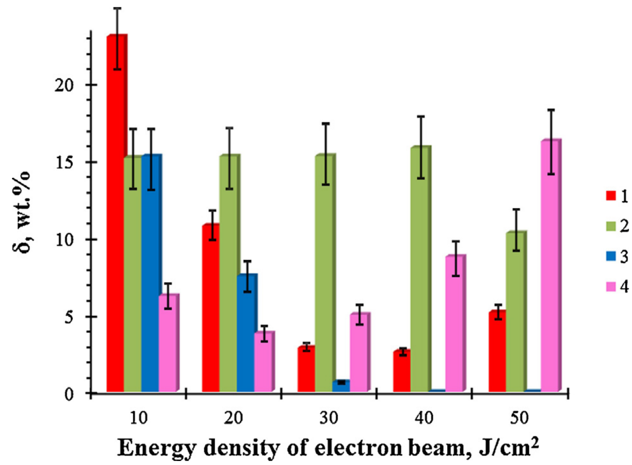

Fig. 8 – Percentage of silicon (Curve 1 and Curve 2) and intermetallic compounds (Curve 3 and Curve 4) in the silumin surface irradiated by an electron beam (1, 3 – pulse time 200 μs; 2, 4 – 50 μs) vs. beam energy density.

Cu_9Al_4. The irradiation of silumin by a pulsed electron beam is related to the transformation of a phase composition in the surface layer. For instance, a percentage of a solid Al-based solution in irradiated samples (pulse time – 200 μs) increases (Fig. 7, Curve 1), whereas it drops in samples irradiated by an electron beam (pulse time −50 μs) (Fig. 7, Curve 2) given that a beam energy density is raised.

Simultaneously, the content and element composition of reinforcing particles tend to change in the surface of irradiated material. As seen in Fig. 8, a percentage of silicon decreases in combination with a rising energy density (a pulse time of an electron beam 200 μs), being minimal at an energy density of 30 J/cm^2 (Fig. 8, Curve 1).

An aggregate percentage of intermetallic compounds (Cu_9Al_4, $Cu_{8.92}Al_{4.08}$, $Cu_{5.64}Al_{4.61}$) also falls, coming up to its zero value at an energy density of 50 J/cm^2 (Fig. 8, Curve 3). For a pulse time of 50 μs the phase composition in the surface layer reverses, i.e. a silicon percentage changes insignificantly in combination with an increasing beam energy density (Fig. 8, Curve 2). An aggregate percentage of intermetallic compounds ($Cu_{8.92}Al_{4.08}$, Cu_7Si_{12}) goes up and comes up to its maximum at an energy density of 50 J/cm^2 (Fig. 8, Curve 4).

The transformation in phase composition and percentage of phases within the electron irradiation of silumin is related to the development of a lattice parameter in the main phase – a solid Al-based solution. It can be seen in Fig. 9a lattice parameter of aluminum changes according to the curve with no regard to a pulse time with a minimum for a pulse time of 200 μs at an energy density of 10 J/cm^2, and for a pulse of 50 μs at an energy density of 30 J/cm^2.

The lattice parameter of aluminum changes principally due to the concentration of alloying elements in the solid solution of the phase. In the literature [4] atomic radii of silicon, copper, nickel, iron, and manganese are bigger than that of aluminum. Therefore, a lattice parameter of aluminum depends on the concentration of these elements in the solid solution. A correlation between aluminum lattice parameter,

Table 2 – Element analysis data of the silumin surface irradiated by a pulsed electron beam (Al – balanced).

Irradiation mode		Element, wt.%				
E_S, J/cm^2	τ, μs	Mg	Si	Fe	Ni	Cu
10	50	1.0 ± 0.09	16.4 ± 1.59	0.27 ± 0.01	1.13 ± 0.11	3.1 ± 0.29
	200	0.79 ± 0.07	17.4 ± 1.70	0.18 ± 0.09	0.94 ± 0.08	2.74 ± 0.27
30	50	0.94 ± 0.08	9.59 ± 0.87	0.25 ± 0.02	0.96 ± 0.09	2.59 ± 0.24
	200	1.19 ± 0.11	8.76 ± 0.83	0.27 ± 0.02	1.22 ± 0.11	3.3 ± 0.33
50	50	0.9 ± 0.08	8.95 ± 0.81	0.21 ± 0.02	0.75 ± 0.07	2.72 ± 0.26
	200	0.86 ± 0.08	9.23 ± 0.83	0.22 ± 0.01	1.2 ± 0.11	2.59 ± 0.28
As delivered		0.87 ± 0.08	17.30 ± 1.71	0.20 ± 0.01	0.84 ± 0.08	2.61 ± 0.25

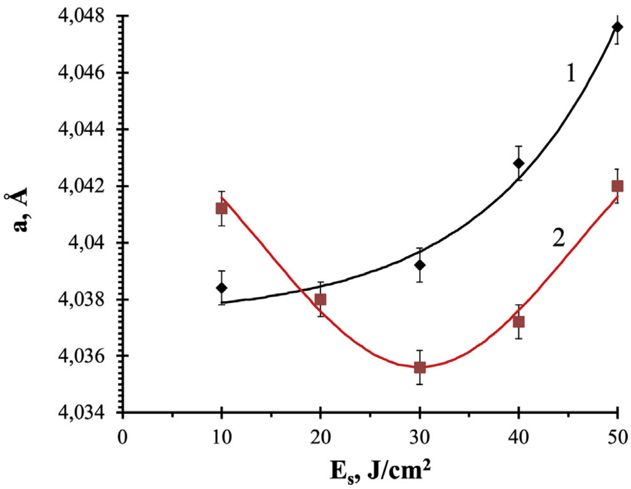

Fig. 9 – Lattice parameter of a solid Al-based solution in the silumin surface irradiated by an electron beam vs. electron beam energy density; 1 – pulse time 200 μs; 2 – 50 μs.

pulse time and energy density of an electron beam will be related to dissolution processes of silicon particles and intermetallic compounds and their re-release to take place when irradiating the material by a pulsed electron beam. To sum up, data presented in Fig. 9 allow a conclusion the saturation of aluminum crystal lattice by alloying and impurity elements (a pulse time 200 μs) is more intensive than at a pulse time of 50 μs.

Relying on outcomes to emerge from the analysis of structure and phase composition in the silumin surface we suggest the hardness of the material increases in conjunction with a pulse time of 50 μs and 200 μs (Fig. 1) as a sub-micro-sized structure of high-speed cellular crystallization forms (Fig. 5, b, d), a solid aluminum-based solution is enriched with alloying and impurity elements, and nano-dimensional particles of reinforcing phases (silicon, intermetallic compounds) re-release.

4. Conclusion

The study has pointed out the microhardness of the surface layer in Al-10wt%Si-2wt%Cu alloy is associated with the electron beam energy density irrespectively to the pulse time (50 μs and 200 μs) and comes to its maximal value, which is more than 1.6 times higher than that in the as delivered material at $E_S = 30–40\,J/cm^2$. The irradiation of silumin by an intensive electron beam (energy density $10\,J/cm^2$) is related to the intensive destruction and microcracking along grain boundaries to contain particles of intermetallic compounds, as well as to the globularization of eutectic cementite lamellae. The research has demonstrated the electron beam irradiation of silumin with an energy density of $30–50\,J/cm^2$ whatever the pulse time of a beam is leads to certain outcomes. First, micropores originate in the surface of samples due to the material shrinkage related to the crystallization of a molten layer, second, silicon tends to dissolve and the globularization of intermetallic compounds takes place; finally, a sub-micro-sized crystal structure of high-speed cellular crystallization develops, crystallites in a range 0.3–0.4 μm. The irradiation of silumin by a pulsed electron beam has been established to cause the saturation of an aluminum-based crystal lattice with alloying and impurity elements. Taken into consideration all the research findings, we suggest an increase in the material hardness owing to the electron irradiation is possible because of a sub-micro-sized structure of high-speed cellular crystallization, the enrichment of a solid aluminum-based solution with alloying and impurity elements, and the re-release of nano-dimensional particles of reinforcing phases (silicon and intermetallic compounds).

Conflicts of interest

The authors declare no conflict of interest.

Acknowledgements

The research was financially supported by the Russian Science Foundation (RSF) (project № 19-79-10059).

REFERENCES

[1] Guan QF, Zou H, Zou GT, Wu AM, Hao SZ, Zou JX, et al. Surface nanostructure and amorphous state of a low carbon steel induced by high-current pulsed electron beam. Surf Coat Technol 2005;196:145–9, http://dx.doi.org/10.1016/j.surfcoat.2004.08.104.

[2] Guo G, Tang G, Ma X, Sun M, Ozur GE. Effect of high current pulsed electron beam irradiation on wear and corrosion resistance of Ti6Al4V. Surf Coat Technol 2013;229:140–5, http://dx.doi.org/10.1016/j.surfcoat.2012.08.009.

[3] Walker JC, Murray JW, Nie M, Cook RB, Clare AT. The effect of large-area pulsed electron beam melting on the corrosion and microstructure of a Ti6Al4V alloy. Appl Surf Sci 2014;311:534–40, http://dx.doi.org/10.1016/j.apsusc.2014.05.105.

[4] Hao Y, Gao B, Tu GF, Li SW, Dong C, Zhang ZG. Improved wear resistance of Al–15Si alloy with a high current pulsed electron beam treatment. Nucl Instrum Methods Phys Res Sect B Beam Interact Mater Atoms 2011;269:1499–505, http://dx.doi.org/10.1016/j.nimb.2011.04.010.

[5] Zhang C, Lv P, Xia H, Yang Z, Konovalov S, Chen X, et al. The microstructure and properties of nanostructured Cr-Al alloying layer fabricated by high-current pulsed electron beam. Vacuum 2019;167:263–70, http://dx.doi.org/10.1016/j.vacuum.2019.06.022.

[6] Hao Y, Gao B, Tu GF, Li SW, Hao SZ, Dong C. Surface modification of Al–20Si alloy by high current pulsed electron beam. Appl Surf Sci 2011;257:3913–9, http://dx.doi.org/10.1016/j.apsusc.2010.11.118.

[7] Liu K, Chen X, Shen Q, Pan Z, Singh RA, Jayalakshmi S, et al. Microstructural evolution and mechanical properties of deep cryogenic treated Cu–Al–Si alloy fabricated by Cold Metal Transfer (CMT) process. Mater Charact 2020;159:110011, http://dx.doi.org/10.1016/j.matchar.2019.110011.

[8] Hao SZ, Zhang Y, Xu Y, Gey N, Grosdidier T, Dong C. WC/Co composite surface structure and nano graphite precipitate induced by high current pulsed electron beam irradiation. Appl Surf Sci 2013;285:552–6, http://dx.doi.org/10.1016/j.apsusc.2013.08.092.

[9] Murray JW, Walker JC, Clare AT. Nanostructures in austenitic steel after EDM and pulsed electron beam irradiation. Surf

Coat Technol 2014;259:465–72, http://dx.doi.org/10.1016/j.surfcoat.2014.10.045.
[10] Luo D, Tang G, Ma X, Gu L, Sun M, Wang L. Various categories of defects after surface alloying induced by high current pulsed electron beam irradiation. Appl Surf Sci 2015;351:1069–74, http://dx.doi.org/10.1016/j.apsusc.2015.06.014.
[11] Cai J, Guan Q, Lv P, Zhang C, Yin Y. Crater formation on the surface of pure metal and alloy irradiated by high current pulsed electron beam. High Temp Mater Process 2018;37:777–84, http://dx.doi.org/10.1515/htmp-2017-0067.
[12] Cai J, Ji L, Yang S, Wang X, Li Y, Hou X, et al. Deformation mechanism and microstructures on polycrystalline aluminum induced by high-current pulsed electron beam. Chin Sci Bull 2013;58:2507–11, http://dx.doi.org/10.1007/s11434-013-5848-5.
[13] Cai Y, Zhang K, Zhang Z, Dong J, Lei Y, Zhang T. Surface nanostructure formations in an AISI 316L stainless steel induced by pulsed electron beam treatment. J Nanomater 2015;2015:1–5, http://dx.doi.org/10.1155/2015/796895.
[14] Tang G, Luo D, Fan G, Ma X, Wang L. Strengthening effect of nano-scaled precipitates in Ta alloying layer induced by high current pulsed electron beam. Nucl Instrum Methods Phys Res Sect B Beam Interact Mater Atoms 2017;398:9–12, http://dx.doi.org/10.1016/j.nimb.2017.03.026.
[15] Li MC, Hao SZ, Wen H, Huang RF. Surface composite nanostructures of AZ91 magnesium alloy induced by high current pulsed electron beam treatment. Appl Surf Sci 2014;303:350–3, http://dx.doi.org/10.1016/j.apsusc.2014.03.004.
[16] Han Z, Han J, Jing Z. Surface microstructure of nanoaluminized CoCrAlY coating irradiated by HCPEB. J Nanomater 2016;2016:1–8, http://dx.doi.org/10.1155/2016/7124218.
[17] Yan P, Grosdidier T, Zhang X, Zou J. Formation of large grains by epitaxial and abnormal growth at the surface of pulsed electron beam treated metallic samples. Mater Des 2018;159:1–10, http://dx.doi.org/10.1016/j.matdes.2018.08.033.
[18] Samih Y, Marcos G, Stein N, Allain N, Fleury E, Dong C, et al. Microstructure modifications and associated hardness and corrosion improvements in the AISI 420 martensitic stainless steel treated by high current pulsed electron beam (HCPEB). Surf Coat Technol 2014;259:737–45, http://dx.doi.org/10.1016/j.surfcoat.2014.09.065.
[19] Fetzer R, Mueller G, An W, Weisenburger A. Metal surface layers after pulsed electron beam treatment. Surf Coat Technol 2014;258:549–56, http://dx.doi.org/10.1016/j.surfcoat.2014.08.039.
[20] An W, Krasik YE, Fetzer R, Bazylev B, Mueller G, Weisenburger A, et al. Characterization of high-current electron beam interaction with metal targets. J Appl Phys 2011;110:093304, http://dx.doi.org/10.1063/1.3660764.
[21] Lu G, Li J, Zhang Y, Sokol DW. A metal marking method based on laser shock processing. Mater Manuf Process 2019;34(6):598–603, http://dx.doi.org/10.1080/10426914.2019.1566618.
[22] Maruschak P, Zakiev I, Mocharsky V, Nikiforov Y. Experimental study of the surface of steel 15Kh13MF after the nanosecond laser shock processing. Solid State Phenom 2013;200:60–5, http://dx.doi.org/10.4028/www.scientific.net/SSP.200.60.
[23] Okipnyi IB, Maruschak PO, Zakiev VI, Mocharskyi VS. Fracture mechanism analysis of the heat-resistant steel 15Kh2MFA(II) after laser shock-wave processing. J Fail Anal Prev 2014;14(5):668–74, http://dx.doi.org/10.1007/s11668-014-9869-4.
[24] Wei X, Ling X, Zhang M. Influence of surface modifications by laser shock processing on the acid chloride stress corrosion cracking susceptibility of AISI 304 stainless steel. Eng Fail Anal 2018;91:165–71, http://dx.doi.org/10.1016/j.engfailanal.2018.04.045.
[25] Regulski K, Wilk-Kołodziejczyk D, Szymczak T, Gumienny G, Pirowski Z, Jaśkowiec K, et al. Data mining methods for prediction of multi-component Al-Si alloy properties based on cooling curves. J Mater Eng Perform 2019;28:7431–44, http://dx.doi.org/10.1007/s11665-019-04442-z.
[26] Kuz'min MP, Larionov LM, Kondratiev VV, Kuz'mina MY, Grigoriev VG, Knizhnik AV, et al. Fabrication of silumins using silicon production waste. Russ J Non-Ferrous Met 2019;60:483–91, http://dx.doi.org/10.3103/S1067821219050122.
[27] Jiang B, Ji Z, Hu M, Xu H, Xu S. A novel modifier on eutectic Si and mechanical properties of Al-Si alloy. Mater Lett 2019;239:13–6, http://dx.doi.org/10.1016/j.matlet.2018.12.045.
[28] Baranov VN, Deev VB, Partyko EG, Belyaev SV, Yur'ev PO, Prusov ES. Influence of atomic and molecular hydrogen in silumins melts on their mechanical properties. Metallurgist 2019;63:521–8, http://dx.doi.org/10.1007/s11015-019-00852-5.
[29] Zheng Z, Ji Y, Mao W, Yue R, Liu Z. Influence of rheo-diecasting processing parameters on microstructure and mechanical properties of hypereutectic Al–30%Si alloy. Trans Nonferrous Met Soc China 2017;27:1264–72, http://dx.doi.org/10.1016/S1003-6326(17)60147-X.
[30] Piątkowski J, Wieszała R. Crystallization and structure of AlSi10Mg0.5Mn0.5 alloy with dispersion strengthening with Al–FexAly–SiC phases. Metals (Basel) 2019;9:865, http://dx.doi.org/10.3390/met9080865.
[31] Sigworth G, Campbell J, Jorstad J. The modification of Al-Si casting alloys: important practical and theoretical aspects. Int J Met 2009;3:65–78, http://dx.doi.org/10.1007/BF03355442.
[32] Ozur GE, Proskurovsky DI, Karlik KV. A wide-aperture, low-energy, and high-current electron beam source with a plasma anode based on a reflective discharge. Instrum Exp Tech 2005;48:753–60, http://dx.doi.org/10.1007/s10786-005-0136-5.
[33] Ozur GE, Proskurovsky DI, Rotshtein VP, Markov AB. Production and application of low-energy, high-current electron beams. Laser Part Beams 2003;21:157–74, http://dx.doi.org/10.1017/S0263034603212040.
[34] Zagulyaev D, Konovalov S, Gromov V, Glezer A, Ivanov Y, Sundeev R. Structure and properties changes of Al-Si alloy treated by pulsed electron beam. Mater Lett 2018;229:377–80, http://dx.doi.org/10.1016/j.matlet.2018.07.064.
[35] Zaguliaev D, Konovalov S, Ivanov Y, Gromov V, Petrikova E. Microstructure and mechanical properties of doped and electron-beam treated surface of hypereutectic Al-11.1%Si alloy. J Mater Res Technol 2019;8:3835–42, http://dx.doi.org/10.1016/j.jmrt.2019.06.045.
[36] Ivanov YF, Gromov VE, Konovalov SV, Zagulyaev DV, Petrikova EA, Semin AP. Modification of structure and surface properties of hypoeutectic silumin by intense pulse electron beams. Usp Fiz Met 2018;19:195–222, http://dx.doi.org/10.15407/ufm.19.02.195.